

Structure and evolution of rotationally and tidally distorted stars

H.F. Song^{1,2,*} Z. Zhong¹ and Y.Lu¹

¹ College of science, Guizhou University, Guiyang, 550025, P.R. China
e-mail: sci.hfsong@gzu.edu.cn, zhongzhen307@yahoo.cn

² Joint Centre for Astronomy, National Astronomical Observatories-Guizhou University, Guiyang, 550025, P.R. China
e-mail: songhanfeng@163.com

ABSTRACT

Aims. This paper aims to study the configuration of two components caused by rotational and tidal distortions in the model of a binary system.

Methods. The potentials of the two distorted components can be approximated to 2nd-degree harmonics. Furthermore, both the accretion luminosity (σ_i) and the irradiative luminosity are included in stellar structure equations.

Results. The equilibrium structure of rotationally and tidally distorted star is exactly a triaxial ellipsoids. A formula describing the isobars is presented, and the rotational velocity and the gravitational acceleration at the primary surface simulated. The results show the distortion at the outer layers of the primary increases with temporal variation and system evolution. Besides, it was observed that the luminosity accretion is unstable, and the curve of the energy-generation rate fluctuates after the main sequence in rotation sequences. The luminosity in rotation sequences is slightly weaker than that in non-rotation sequences. As a result, the volume expands slowly. Polar ejection is intensified by the tidal effect. The ejection of an equatorial ring may be favoured by both the opacity effect and the $g_e(\theta, \varphi)$ -effect in the binary system.

Key words. star, stellar rotation, evolution

1. Introduction

In the conventional model of binary stars, there is no consideration of spin and tidal effects (Eggleton 1971,1972,1973; Hofmeister, Kippenhahn & Weigert, 1964; Kippenhahn et al. 1967; etc.); however, rotation and tide have been regarded as two important physical factors in recent years, so they need to be considered for a better understanding of the evolution of massive close binaries (e.g., Heger, Langer & Woosley 2000a; Meynet & Maeder 2000). The structure and evolution of rotating single stars has been studied by many investigators (Kippenhahn & Thomas 1970; Endal & Sofia 1976; Pinsonneault et al. 1989; Meynet & Maeder 1997; Langer 1998, 1999; Huang 2004a). However, it is also very important to study the evolution of rotating binary stars (Jackson 1970; Chan & Chau 1979; Langer 2003; Huang 2004b; Petrovic et al 2005a,b; Yoon et al. 2006). The effect of spin on structure equations has been investigated (e.g. the present Eggleton's stellar evolution code; Li et al 2004a,b, 2005; Kähler 2002). They adopted the lowest-order approximate analysis in which two components were treated as spherical stars. In fact, with the joint effects of spin and tide, the structure of a star changes from spherically symmetric to non-spherically symmetric. Then, the stellar structure equations become three dimensional. Theory distinguishes two components in the tide, namely equilibrium tide (Zahn 1966) and the dynamical tide (Zahn 1975). Then, the dissipation mechanisms acting on those tides, namely the viscous friction for the equilibrium tide and the radiative damping for the dynamical tide, have been identified (Zahn 1966, 1975, 1977). The distortion throughout the outer regions of the two components is not small in short-

period binary systems. The higher-order terms in the external gravitational field should not be ignored (Jackson 1970).

It is a very complex process to determine the equilibrium structure of the two components. Therefore, approximate methods have been widely adopted for studying these effects. In 1933, the theory of distorted polytropes was introduced by Chandrasekhar. Kopal (1972,1974) developed the concept of Roche equipotential and of Roche coordinates to analyse the problem of rotationally and tidally distorted stars in a binary system. Burša (1989a,1988) took advantage of the high-order perturbing potential to describe rotational and tidal deformations to discuss the figures and dynamic parameters of synchronously orbiting satellites in the solar system. The equilibrium structure of the two components were treated as two non-symmetric rotational ellipsoids with two different semi-major axes a_1 and a_2 ($a_1 > a_2$) by Huang (2004b). It is very important that Kippenhahn & Thomas (1970) introduced a method of simplifying the two-dimensional model with conservative rotation and allowed the structure equations for a one-dimensional star to incorporate the hydrostatic effect of rotation. This method has been adopted by Endal & Sofia (1976) and Meynet & Maeder (1997), who applied it to the case of shellular rotation law (Zahn 1992). In this case, the rotation rate takes the simplified form of $\Omega = \Omega(r)$. It was demonstrated that the shape of an isobar in the case of the shellular rotation law is identical to one of the equipotentials in the conservative case of Meynet & Maeder (1997).

At the semi-detached stage, both mass transfer between the components and luminosity change of a secondary exist due to the release of accretion energy which is correlative with the external potential of the two components. When the joint effect of rotation and tide are considered, the potential of the two components are different from those in non-rotational cases. Therefore, the luminosity due to the release of accretion energy, as well

* Send offprint requests to: H. F. Song, e-mail: sci.hfsong@gzu.edu.cn

as irradiation energy, can significantly alter the structure and evolution of the secondary. In a rotating star, meridional circulation and shear turbulence exist, both of which can drive the transport of chemical elements. This effect is stronger and has already been studied by many scholars (Endal & Sofia 1978; Pinsonneault et al. 1989; Chaboyer & Zahn 1992; Zahn 1992; Meynet & Maeder 1997; Maeder 1997; Meader & Zahn 1998; Maeder & Meynet 2000; Denissenkov et al. 1999; Talon et al. 1997; Decressin et al. 2009). In this paper, the amplitude expression for the radial component of the meridional circulation velocity $U(r)$ considers the effect of tidal force, which may be important in a massive close binary system.

This paper is divided into four main sections. In section 2, the structure equations of rotating binary stars are presented. Material diffusion equations and boundary conditions are provided. Then, the accretion luminosity, including gravitational energy, heat energy, and radiation energy, is deduced. In section 3, the results of numerical calculation are described and discussed in detail. In section 4, conclusions are drawn.

2. Model for rotating binary stars

2.1. Potential of rotating binary stars

It is well known that the rotation of a component is synchronous with the orbital motion of a system thanks to a strong tidal effect. Such synchronous rotation also exists inside the component (Giuricin et al. 1984; Van Hamme & Wilson 1990); therefore, conventional theories usually assume that two components rotate synchronously and revolve in circular orbits (Kippenhahn & Weigert 1967; De Loore 1980; Huang & Taam 1990; Vanbeveren 1991; De Greve 1993). A coordinate system rotating with the orbital angular velocity of the stars is introduced. The mass centre of the primary is regarded as the origin, and it is presumed that the z -axis is perpendicular to the orbital plane, and the positive x -axis penetrates the mass centre of the secondary. The gravitational potential at any point $P(r, \theta, \varphi)$ of the surface of the primary can be approximately expressed as

$$\Psi = V + \frac{1}{3}\Omega^2 r^2 (1 - P_2(\cos\theta)) + V_t, \quad (1)$$

where V is the gravitational potential and given by Burše (1989a, 1988),

$$V = \frac{GM_1}{r_p} \left[\frac{r_p}{r} + \left(\frac{r_p}{r}\right)^3 J_2^{(0)} P_2^0(\cos\theta) + \left(\frac{r_p}{r}\right)^3 J_2^{(2)} P_2^2(\cos\theta) \cos 2\varphi \right]. \quad (2)$$

Here, V_t is the tidal potential (Burše 1989a)

$$V_t = \frac{GM_2}{D} \left(\frac{r}{D}\right)^2 \left[-\frac{1}{2} P_2^0(\cos\theta) + \frac{1}{4} P_2^2(\cos\theta) \cos 2\varphi \right], \quad (3)$$

where it is assumed that the mean equatorial radius equals that of the equivalent sphere in the above equation for the convenience of calculation. Both M_1 and M_2 are the mass of the primary and the secondary, respectively, and r_p represents each equivalent radius inside the star, $P_2^2(\cos\theta)$ and $P_2^0(\cos\theta)$ are the associated Legendre function ($P_2^0(\cos\theta) = \frac{3}{2} \cos^2\theta - \frac{1}{2}$, $P_2^2(\cos\theta) = 3 \sin^2\theta$), D is the distance between the two components, and Ω is the orbital angular velocity of the system. It can be represented by

$$\Omega^2 = G(M_1 + M_2)/D^3, \quad (4)$$

where $J_2^{(0)}$ and $J_2^{(2)}$ are dimensionless stokes parameters. If M_1 can generally be negligible compared to M_2 , the stokes parameters can be expressed as (Burše 1989a, 1988)

$$J_2^{(0)} = -\left[\frac{1}{3}k_s + \frac{1}{2}k_t\right]q\left(\frac{r_p}{D}\right)^3 = -J_2, \quad (5)$$

$$J_2^{(2)} = \frac{1}{4}k_t q \left(\frac{r_p}{D}\right)^3, \quad (6)$$

where k_s is the secular Love number, which is expressed as a measure of the body-yeild-to-centrifugal deformation, and k_t is an analogous parameter that is introduced to describe the secular tidal deformations. The response of the body to its centrifugal acceleration and to the tidal perturbing potential is different in the usual case. Therefore, the body-yeild-to centrifugal deformation is not equal to the body-yeild-to-tidal deformation. If the subject investigated is regarded as an ideal elastic body, the body-yeild-to centrifugal deformation is equal to the body-yeild-to-tidal deformation, $k_s = k_t$. In the ideal static equilibrium, $k_s = k_t = 1$ (Burše 1989a). We assume the ideal static equilibrium in this paper. q is the mass ratio of the secondary to the primary ($q = \frac{M_2}{M_1}$). With Eqs. (2) and (3) being combined with Eq. (1), the potential of the primary can be obtained as

$$\begin{aligned} \Psi_P = & \frac{GM_1}{D} \left\{ \frac{D}{r_1} + \frac{1}{2} \frac{D}{r_1} \left(\frac{r_p}{r_1}\right)^2 \right\} [-J_2(3 \cos^2\theta - 1) \\ & + 6J_2^{(2)} \sin^2\theta \cos 2\varphi] + \frac{1}{2}(1+q)\left(\frac{r_1}{D}\right)^2 \sin^2\theta \\ & + \frac{1}{4}q\left(\frac{r_1}{D}\right)^2 [3 \sin^2\theta (1 + \cos 2\varphi) - 2], \end{aligned} \quad (7)$$

The potential of the secondary is deduced by substituting M_2 for M_1 and $\frac{1}{q}$ for q . The isobar defined by the equation $P = const$ is assumed to be a triaxial ellipsoid with three semi-major axes: a , b , and c . The shortest axis defined by c is identical to its rotational axis and perpendicular to its orbital plane. The longest axis defined by a is identical with its x -axis.

2.2. Considering stellar structure equations with spin and tidal effects

The spin of the two components is rigid rotation, and it belongs to conservative rotation. The definition of equivalent sphere was adopted in a practical calculation. Therefore, the triaxial ellipsoid model is simplified to a one-dimensional model. The structure equations are presented as

$$\frac{\partial r_P}{\partial M_P} = \frac{1}{4\pi r_P^2 \rho}, \quad (8)$$

$$\frac{\partial P}{\partial M_P} = -\frac{GM_P}{4\pi r_P^4} f_P, \quad (9)$$

$$\frac{\partial L_P}{\partial M_P} = \varepsilon_N - \varepsilon_V + \varepsilon_g + \sigma_{ac}, \quad (10)$$

where σ_{ac} is the energy source per unit mass caused by mass overflow and irradiation. Because accretion luminosity is caused by energy sources in the gainer's outermost layer, there exists

$$\sigma_{ac} \Delta m = \Delta L_{acc}, \quad (11)$$

where Δm is the photosphere mass of the secondary. The surface temperature of the secondary may be approximated by the formula, $L_2 + \Delta L_{acc} = 4\pi R_2^2 \sigma T_{eff}^4$, where L_2 is the luminosity coming to the photosphere from the stellar interior, and σ is the Stefan-Boltzmann constant:

$$\frac{d \ln T}{d \ln P} = \begin{cases} \nabla_{RfT}/f_p \\ \nabla_{con} \end{cases} \quad (12)$$

$$f_P = \frac{4\pi r_p^4}{GM_p S_p} \frac{1}{\langle g_{eff}^{-1} \rangle}, \quad (13)$$

$$f_T = \frac{4\pi r_p^2}{S_p} \frac{1}{\langle g_{eff} \rangle \langle g_{eff}^{-1} \rangle}, \quad (14)$$

$$\nabla_R = \frac{3}{16\pi acG} \frac{\kappa LP}{M_p T^4}, \quad (15)$$

where $\langle g_{eff} \rangle$ and $\langle g_{eff}^{-1} \rangle$ are the mean values of effective gravity and its opposites over the isobar surface, and ∇_R is the radiative temperature gradient. The factors f_P and f_T depend on the shape of the isobars.

2.3. Calculation of quantities f_P and f_T

2.3.1. Shape and gravitational acceleration of triaxial ellipsoid

To obtain the factors f_P and f_T , the mean values $\langle g_{eff} \rangle$ and $\langle g_{eff}^{-1} \rangle$ over the isobar surface have to be calculated. Therefore, the shape of isobars must be given first. The functions for the semi-major axes a , b , and c to the radius of the equivalent sphere r_p can be obtained from Eq. (7) as

$$\frac{4\pi abc}{3} = \frac{4\pi r_p^3}{3}, \quad (16)$$

$$\begin{aligned} \frac{GM_1}{D} \left[\frac{D}{a} + \frac{1}{2} \frac{D}{a} \left(\frac{r_p}{a} \right)^2 (J_2 + 6J_2^{(2)}) \right] + \\ \frac{1}{2} (1+q) \left(\frac{a}{D} \right)^2 + q \left(\frac{a}{D} \right)^2 = \frac{GM_1}{D} \left[\frac{D}{c} + \frac{1}{2} \frac{D}{c} \left(\frac{r_p}{c} \right)^2 (-2J_2) \right. \\ \left. - \frac{1}{2} q \left(\frac{c}{D} \right)^2 \right], \end{aligned} \quad (17)$$

$$\begin{aligned} \frac{GM_1}{D} \left[\frac{D}{b} + \frac{1}{2} \frac{D}{b} \left(\frac{r_p}{b} \right)^2 (J_2 - 6J_2^{(2)}) + \frac{1}{2} (1+q) \left(\frac{b}{D} \right)^2 \right. \\ \left. - \frac{1}{2} q \left(\frac{b}{D} \right)^2 \right] = \frac{GM_1}{D} \left[\frac{D}{c} + \frac{1}{2} \frac{D}{c} \left(\frac{r_p}{c} \right)^2 (-2J_2) \right. \\ \left. - \frac{1}{2} q \left(\frac{c}{D} \right)^2 \right]. \end{aligned} \quad (18)$$

The left hand side of Eq.(17) corresponds to $\theta = \frac{\pi}{2}$ and $\varphi = 0$, while the one of Eq.(18) corresponds to $\theta = \frac{\pi}{2}$ and $\varphi = \frac{\pi}{2}$. The three semi-major axes a , b , and c of a triaxial ellipsoid can be obtained numerically by solving (16), (17), and (18). From (7), the quantities g_r , g_θ , and g_φ at the surface of the two components take the forms of

$$\begin{aligned} g_r = -\frac{\partial \Psi}{\partial r} = \frac{GM_1}{D^2} \left\{ \left(\frac{D}{r} \right)^2 + \frac{3}{2} \frac{D^2}{r^2} \left(\frac{r_p}{r} \right)^2 \right. \\ \left. [-J_2(3 \cos^2 \theta - 1) + 6J_2^{(2)} \sin^2 \theta \cos 2\varphi] - \frac{r}{D} (1+q) \sin^2 \theta \right. \\ \left. - \frac{r}{D} q (3 \sin^2 \theta \cos^2 \varphi - 1) \right\}, \end{aligned} \quad (19)$$

$$\begin{aligned} g_\theta = -\frac{1}{r} \frac{\partial \Psi}{\partial \theta} = \frac{GM_1}{D^2} \left\{ -\frac{D^2}{r^2} \left(\frac{r_p}{r} \right)^2 [3J_2 + 6J_2^{(2)} \right. \\ \left. (2 \cos^2 \varphi - 1)] - (1+q) \frac{r}{D} - 3q \frac{r}{D} \cos^2 \varphi \right\} \sin \theta \cos \theta, \end{aligned} \quad (20)$$

$$\begin{aligned} g_\varphi = -\frac{1}{r \sin \theta} \frac{\partial \Psi}{\partial \varphi} \\ = \frac{GM_1}{D^2} [12 \left(\frac{D}{r} \right)^2 \left(\frac{r_p}{r} \right)^2 J_2^{(2)} + 3q \frac{r}{D}] \sin \theta \cos \varphi \sin \varphi. \end{aligned} \quad (21)$$

However, the total potential in the stellar interior (to first-order approximation) can be composed by four parts (Kopal 1959, 1960, 1974; Endal & Sofia 1976 and Landin 2009): ψ_s , the spherical symmetric part of the gravitational potential; ψ_r ,

the cylindrically symmetric potential due to rotation; ψ_t the non-symmetric potential due to tidal force, and ψ_d , the non-symmetric part of the gravitational potential due to the distortion of the component considering the rotational and tidal effects. Therefore, the total potential at $P(r, \theta, \varphi)$ is

$$\begin{aligned} \Psi = \psi_s + \psi_r + \psi_t + \psi_d \\ = \frac{GM_\psi}{r} + \frac{1}{2} \omega^2 r^2 \sin^2 \theta + \frac{GM_2}{D} \left[1 + \sum_{j=2}^4 \left(\frac{r_0}{D} \right)^j P_j(\sin \theta \cos \varphi) \right] \\ - \frac{4\pi}{3r^3} P_2(\cos \theta) \int_0^{r_0} \rho \frac{r_0'^7}{M_\psi} \Omega^2 \frac{5 + \eta_2}{2 + \eta_2} dr_0' \\ + 4\pi GM_2 \sum_{j=2}^4 \frac{P_j(\sin \theta \cos \varphi)}{(rD)^{j+1}} \int_0^{r_0} \rho \frac{r_0'^{2j+3}}{M_\psi} \frac{j+3 + \eta_j}{j + \eta_j} dr_0'. \end{aligned} \quad (22)$$

The quantity η_j can be evaluated by numerically integrating the Radau's equation (cf. Kopal 1959)

$$r_0 \frac{d\eta_j}{dr_0} + 6 \frac{\rho(r_0)}{\bar{\rho}(r_0)} (\eta_j + 1) + \eta_j (\eta_j - 1) = j(j+1), \quad (23)$$

for $j=2,3,4$, and boundary condition $\eta_j(0) = j-2$. The quantity r_0 is the mean radius of the corresponding isobar. The local effective gravity is given by differentiation of the total potential and is written as

$$g_i = \left[\left(\frac{\partial \Psi}{\partial r} \right)^2 + \left(\frac{1}{r} \frac{\partial \Psi}{\partial \theta} \right)^2 + \left(\frac{1}{r \sin \theta} \frac{\partial \Psi}{\partial \varphi} \right)^2 \right]^{\frac{1}{2}}, \quad (i = 1, 2). \quad (24)$$

The integral in above equations and their derivatives must be evaluated numerically. The mean values of g_{effi} and g_{effi}^{-1} over the surfaces of the triaxial ellipsoids can be obtained as

$$\langle g_{effi} \rangle = \frac{1}{S_P} \int_0^\pi \int_0^{2\pi} g_{effi} r_i^2 \sin \theta d\theta d\varphi, \quad (i = 1, 2) \quad (25)$$

$$\langle g_{effi}^{-1} \rangle = \frac{1}{S_P} \int_0^\pi \int_0^{2\pi} g_{effi}^{-1} r_i^2 \sin \theta d\theta d\varphi, \quad (i = 1, 2). \quad (26)$$

According to Eqs. (13) and (14), the values of f_P and f_T can be obtained when the mean values $\langle g_{eff} \rangle$ and $\langle g_{eff}^{-1} \rangle$ are known. r_1 and r_2 are the distances between the centre of the components and the surfaces of two triaxial ellipsoids. They are

$$r_i^2 = \frac{a_i^2 b_i^2 c_i^2}{b_i^2 c_i^2 \sin^2 \theta \cos^2 \varphi + a_i^2 c_i^2 \sin^2 \theta \sin^2 \varphi + a_i^2 b_i^2 \cos^2 \theta}, \quad (i = 1, 2). \quad (27)$$

The surface area S_p of the isobar can be expressed as

$$S_p = \frac{4\pi}{3} (a^2 + b^2 + c^2). \quad (28)$$

2.4. Element diffusion process

The effect of meridian circulation can drive the transport of chemical elements and angular momentum in rotating stars. For the components in solid-body rotation, no differential rotation exists that can cause shear turbulence. According to Endal & Sofia (1978) and Pinsonneault (1989), the transport of chemical composition is treated as a diffusion process. The equation takes the form of (Chaboyer & Zahn 1992)

$$\left(\frac{\partial y_\alpha}{\partial t} \right) = \frac{1}{\rho r^2} \frac{\partial}{\partial r} \left[\rho r^2 D_{dif} \left(\frac{\partial y_\alpha}{\partial r} \right) \right] + \left(\frac{\partial y_\alpha}{\partial t} \right)_{nuc}, \quad (29)$$

where $(\frac{\partial y_\alpha}{\partial t})_{nuc}$ is a source term from nuclear reactions, and y_α is the relative abundance of α -th nuclide. The diffusion coefficient D_{dif} given by Heger, Langer & Woosley (2000a) can be expressed as

$$D_{dif} \equiv \min\{d_{inst}, H_{v,ES}\}U(r), \quad (30)$$

where d_{inst} and $H_{v,ES}$ denote the extent of the instability and the velocity scale height, respectively. The expression for the amplitude of the radial component of the meridional circulation velocity $U(r)$ (derived from Kippenhahn & Weight 1990) has been modified to take the effects of radiation pressure and tidal force into-account, which are important in a massive close binary system. It is noticed that

$$U(r) = \frac{8}{3} \left(\frac{\Omega^2 r^3}{GM_r} + \frac{GM_2 r^3}{GM_r D^3} \right) \frac{L_r}{g_r M_r} \frac{\gamma-1}{\gamma} \frac{1}{\nabla_{ad}-\nabla} \left(1 - \frac{\Omega^2}{2\pi G \rho} - \frac{\varepsilon}{\varepsilon_m} \right) \quad (31)$$

where the term $\frac{\Omega^2 r^3}{GM_r} + \frac{M_2 r^3}{M_r D^3}$ is the local ratio of centrifugal force and tidal force to gravity, γ is the ratio of the specific heats $\frac{C_p}{C_v}$, L_r represents the luminosity at radius r , M_r is the mass enclosed within a sphere of radius r , ∇ is the actual gradient and ∇_{ad} is adiabatic temperature gradient, $\varepsilon_m = \frac{L}{m}$ gives the mean energy production rate, and ε is local generation rate of nuclear-energy.

There is no source or sink at the inner and the outer boundaries of the two components. Therefore, the boundary conditions are used as

$$\left(\frac{\partial y_\alpha}{\partial r} \right)_{i=1} = 0 = \left(\frac{\partial y_\alpha}{\partial r} \right)_{i=M} \quad (32)$$

where the subscript i denotes different layers inside stars. The initial abundance equals the one at the zero-age main sequence. Therefore, the initial condition is

$$(y_\alpha)_{i|t=0} = (y_\alpha)_{i|limit}. \quad (33)$$

2.5. Luminosity accretion

In the case where the joint effect of rotation and tide is ignored, the two components are spherically symmetric. The star fills its Roche lobe and begins to transfer matter to the companion. However, in the case with the effects of rotation and tide being considered, the components are triaxial ellipsoids. The condition for the mass overflow through Roche lobe flow should be revised as $a_1 = r_{robe}$ (Huang 2004b). It is assumed that the transferred mass is distributed within a thin shell at the surface of the primary before the transfer, and within a thin shell at the surface of the secondary after the transfer. Three forms of energy (including potential energy, heat energy, and radiative energy) are transferred to the secondary. The mass transfer rate is \dot{m} . Two different cases are considered:

a) If the joint effect of rotation and tide is ignored, the accretion luminosity can be expressed directly in terms of the Roche lobe potential at the inner Lagrangian point, Ψ_{L_1} , and at the surface of the secondary Ψ_S (Han & Webbink 1999):

$$\Delta L_P = \dot{m}(\Psi_{L_1} - \Psi_S) = \frac{G\dot{m}M_1}{D} \left[\frac{1}{X_{L_1}/D} + \frac{q}{1-X_{L_1}/D} + \frac{1+q}{2} \left(\frac{X_{L_1}}{D} - \frac{q}{1+q} \right)^2 - \frac{q}{R_2/D} - \frac{1}{1-R_2/D} - \frac{1+q}{2} \left(1 - \frac{R_2}{D} - \frac{q}{1+q} \right)^2 \right], \quad (34)$$

where X_{L_1} is the distance between the primary and L_1 , and R_2 is the radius of the secondary.

b) If the joint effect of rotation and tide is considered, the equilibrium structure of the two components will be treated as

triaxial ellipsoids. The release of potential energy because of the accretion of a mass rate \dot{m} to the secondary is given by

$$\Delta L_P = \dot{m}(\Psi_{L_1} - \Psi_S) = \frac{G\dot{m}M_1}{D} \left[\frac{1}{X_{L_1}/D} + \frac{q}{1-X_{L_1}/D} + \frac{1+q}{2} \left(\frac{X_{L_1}}{D} - \frac{q}{1+q} \right)^2 \right] - \frac{GM_2 \dot{m}}{D} \left[\frac{D}{c_2} + \frac{1}{2} \frac{D}{c_2} \left(\frac{r_p}{c_2} \right)^2 (2J_2^0) - \frac{1}{2} q \left(\frac{c_2}{D} \right)^2 \right], \quad (35)$$

where Ψ_S is the potential of the secondary. Similarly, as the two components have different temperatures, the transmitted thermal energy will be

$$\Delta L_T = \dot{m} \left(\frac{3kT_{eff1}}{2\mu_1 m_p} - \frac{3kT_{eff2}}{2\mu_2 m_p} \right), \quad (36)$$

where T_{eff1} and T_{eff2} represent the effective temperature of the primary and the secondary, respectively, and μ_1 and μ_2 are the mean molecular weights of the primary and the secondary, respectively. m_p refers to proton mass. Because of the irradiation, energy accumulated by the primary and the secondary can be given by (Huang & Taam 1990)

$$\Delta L_{r,1,2} = \frac{1}{2} [1 - (D^2 - R_{1,2}^2)^{1/2} / D] L_{2,1}, \quad (37)$$

where R_1 and R_2 are the radii of the primary and the secondary, and L_1 and L_2 are the luminosities of the primary and the secondary, respectively. The total accretion luminosity is

$$\Delta L_{acc} = \beta \Delta L_{tot} = \beta (\Delta L_P + \Delta L_T + \Delta L_r). \quad (38)$$

Because a part of the total energy may be dissipated dynamically, β is assumed to range from 0.1 to 0.5 (Huang 1993). A value $\beta = 0.3$ is adopted.

3. Results of numerical calculation

The structure and evolution of binary system was traced with the modified version of a stellar structure program, which was developed by Kippenhahn et al., (1967) and has been updated to include mass and energy transfer processes. The calculation method is based on the technique of Kippenhahn and Thomas (1970) and takes advantage of the concept of isobar (Zahn 1992, Meynet and Maeder 1997). Both components of the binary are calculated simultaneously. The initial mass of the system components is set at $9M_\odot$ and $6M_\odot$. The initial chemical composition X equals $X=0.70$, and $Z=0.02$ is adopted for the two components. Similarly, the initial orbital separation between the two components for all sequences is defined as $20.771R_\odot$, so mass transfer via Roche lobe occurs in case A (at the central hydrogen-burning phase of the primary). Two evolutionary sequences corresponding to the evolution with the joint effect of rotation and tide being considered or ignored are calculated. The sequence denoted by case 1 represents the evolution without the effects of rotation and tide being considered, while the sequence denoted by case 2 represents the evolution with the effects of rotation and tide being considered. The calculation of Roche lobe is taken from the study by Huang & Taam (1990). The non-conservative evolution in the two cases was considered. Because the local flux at colatitude θ is proportional to the effective gravity g_e according to Von Zeipel theorem (Maeder 1999), the mass-loss rate due to the stellar winds intensified by tidal, rotational, and irradiative effects is obtained according to Huang & Taam(1990) (cf. Table 1). The angular velocity of the system and the orbital separation between the two components change due to a number of factors: changes in physical processes as

the binary system evolves, including the loss of mass and angular momentum via stellar winds, mass transfer via Roche lobe overflow, exchange of angular momentum between component rotation and the orbital motion of the system caused by tidal effect, and changes in moments of inertia of the components. The changes in the angular velocity of the system and the orbital separation between the two components can be calculated according to Huang & Taam (1990), and the results are listed in Table 1. Other parameters are treated in the same way for two sequences.

The evolution of the binary system proceeded as follows (cf. Table 1). Evolutionary time, orbital period, mass of two stars, luminosities and effective temperature of two stars, central and surface helium mass fraction of the primary, and mean equatorial rotational velocities of two stars are listed in Table 1. Points a, b, c, d, e, and f denote the zero-age main sequence, the beginning of the mass transfer stage, the beginning of H-shell burning, the end of central hydrogen-burning, the beginning of the central helium-burning stage, and the end of calculation, respectively. At the beginning of mass exchange, the luminosity and effective temperature of the primary component decrease rapidly. The secondary accretes $6.174M_{\odot}$ for case 1 and $5.502M_{\odot}$ for case 2 during the mass transfer in case A. Because of this mass gain, the luminosity and the temperature of the secondary go up. When the mass is transferred from the more massive star to the less massive one, the separation between the centres of the two components as well as the orbital period of the system decrease. Some orbital angular momentum is transformed into the spin angular momentum of both components, and this process is crucial to model the spin-up of the accretion star. With mass overflow, the mass of the primary will be less than that of the secondary. When the mass is transferred from the less massive star to the more massive one, the separation between the centres of the two components as well as the orbital period of the system increases. Some spin angular momenta in both of the components are transformed into orbital angular momentum. This physical process results in a longer epilogue after mass transfer.

The equilibrium configuration deviates from spherical symmetry because of the centrifugal forces and tidal forces. And the deviated region mainly lies in the outer layer of a star. In fact, the distorted stellar surface forms the shape of a triaxial ellipsoid. A distorted isobar surface can be expressed as

$$r = r_p[1 + f(r)P_2(\cos\theta) + g(r)P_2^2(\cos\theta)\cos 2\varphi], \quad (39)$$

which corresponds to the form of the disturbing potential (Zahn 1992). The coefficients $f(r)$ and $g(r)$ can be defined as $f(r) = -\frac{C_1\Omega^2}{\pi G\rho} - \frac{C_2M_2}{\pi\rho D^3}$ and $g(r) = \frac{C_2M_2}{2\pi\rho D^3}$. The quantity ρ is the mean density of a star with the mass of M_1 . It was noticed that at the central hydrogen-burning phase, two parameters C_1 and C_2 in Eq. (39) gain the values of 0.703 ± 0.125 and 0.491 ± 0.102 , respectively. This formula indicates that the shapes of the two components vary with the potentials of the centrifugal force and the tidal force. The radial deformation is inversely proportional to the mean density of the component. In order to describe the distortion, the distribution of the surface rotating velocities of the primary is illustrated in Fig. 1. The four panels (a), (b), (c), and (d) correspond to the evolutive time of 0, 2.3386×10^7 , 2.6194×10^7 , 2.6287×10^7 years and corresponding periods of 2.776, 2.760, 2.746, and 2.628 days, respectively. The rotational velocity rates for the peaks of the semi-major axes b and a are $\frac{b}{a} = \frac{v_b}{v_a} = 0.9867, 0.9401, 0.8814, \text{ and } 0.8664$ in four panels, respectively. The results show that the surface deformation is intensified with the evolution and volume-expansion of the primary. The distortion throughout the outer region of the primary

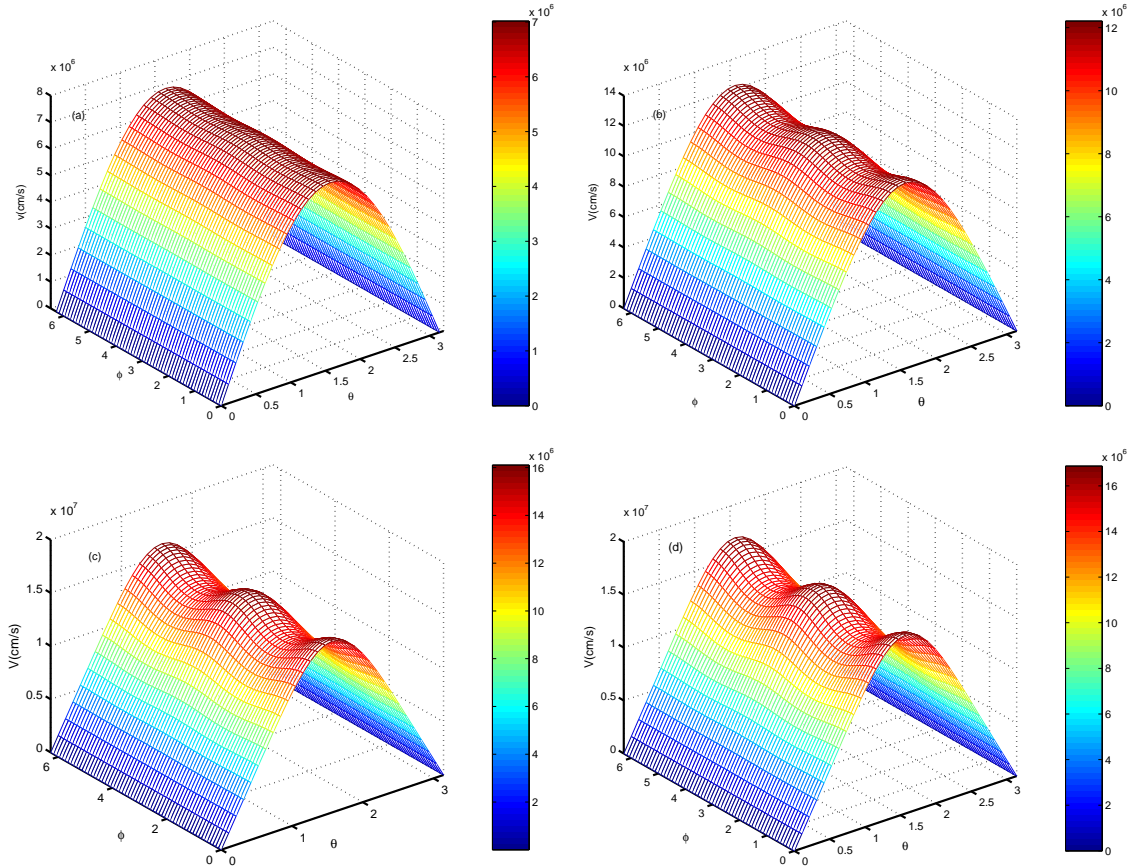
is considerable. The detailed theoretical models that focus on investigation of the outer regions have somewhat deviated from the Roche model. The high-order perturbed potential is required for studying the structure and evolution of short-period binary systems. Matthews & Mathieu (1992) examined 62 spectroscopic binaries with A-type primaries and orbital periods less than 100 days. They concluded that all systems with orbital periods less than or equal to three days have circular orbits or nearly circular orbits. Zahn (1977) and Rieutord & Zahn (1997) have shown how binary synchronization and circularization result from tidal dissipation. Based on smoothed particle hydrodynamics (SPH) simulation, Renvoizé et al.(2002) have quantified the geometrical distortion effect due to the tidal and rotational forces acted on the polytropic secondaries of semi-detached binaries. They suggest that the tidal and rotational distortion on the secondary may not be negligible, for it may reach observable levels of $\sim 10\%$ on the radius in specific cases of polytropic index and mass ratio. Georgy et al.(2008) display that various effects of the rotation on the surface of a $20M_{\odot}$ star at a metallicity of 10^{-5} and at $\sim 95\%$ of the critical rotation velocity. They point out that the star becomes oblate with an equatorial-to-polar radius ratio $\frac{R_{eq}}{R_{pol}} \simeq 1.3$. These results agree closely with ours.

The variation relative gravitational accelerations, the tidal force, and the ratio of f_{cen}/f_{tid} on the surface of the primary under the coordinate θ and φ at the beginning of mass overflow are shown in Fig. 2. The quantities g_r , g_{θ} , and g_{φ} are the three components of gravitational acceleration. The six panels (a), (b), (c), (d), (e), and (f) represent the distribution of g_r/g , g_{θ}/g , g_{φ}/g , g_{tot}/g , f_{tid} , and f_{cen}/f_{tid} , respectively. The quantity g equals the gravitational acceleration of the corresponding equivalent sphere ($g = \frac{GM_1}{r_p^2}$). When the joint effect of rotation and tide is considered, the gravitational accelerations are different from those in the conventional model. Gravitational acceleration generally has three components.

It is shown in panel (a) that the relative quantity $\frac{g_r}{g}$ reaches the maximum value of 1.048 at the two polar points and drops to the minimum value 0.6987 on the equatorial plane because the inward tidal force acts on the primary and causes the polar radius to become shorter. The tidal and centrifugal forces pull the primary outwards and change gravitational accelerations greatly on the equatorial plane. Furthermore, the maximum value is 0.9486 and the minimum value is 0.6987 on the equatorial plane. The lower values are at the peak of the longest axis a and the higher values are at the peak of the axis b . The relative quantity $\frac{g_{\theta}}{g}$ reaches the maximum value of 0.20399 at the point of $\theta = \frac{k\pi}{2} + \frac{\pi}{4}; \varphi = k\pi, k = 0, 1$ and vanishes at the two polar points and on the equatorial plane in panel (b). It can be seen that a secondary maximal value of 0.10214 exists at point of $\theta = \frac{k\pi}{2} + \frac{\pi}{4}; \varphi = k\pi + \frac{\pi}{2}, k = 0, 1$. The relative quantity $\frac{g_{\varphi}}{g}$ reaches the maximum value of 0.1050 at point $\theta = \frac{\pi}{2}; \varphi = \frac{k\pi}{2} + \frac{\pi}{4}, k=0,1,2,3$ and decreases to zero at the point of $\varphi = \frac{k\pi}{2}, k = 0, 1, 2, 3$ in panel (c). The total gravitational acceleration at the surface of the primary is shown in panel (d). Its distribution is similar to the one of $\frac{g_r}{g}$ because the radial component is the maximum value. It is noticed that, as expected, the average gravitational acceleration of the rotating model is less than for the non-rotating model. It can be observed that the tidal force reaches the highest value of 340.05cm/s^2 at the point of $\theta = \frac{\pi}{2}; \varphi = k\pi, k = 0, 1$ and decreases to the lowest of 136.24cm/s^2 at the two polar points. The quantity f_{cen}/f_{tid} reaches the maximum value of 2.4905 at the point of

Table 1. Parameters at different evolutionary points a, b, c, d, e, and f in sequences of cases 1 and 2.

Sequence	Time 10^7 yr	P day	M_1 M_\odot	M_2 M_\odot	$\log L_1/L_\odot$	$\log T_{1,eff}$	$\log L_2/L_\odot$	$\log T_{2,eff}$	$Y_1(c)$	Y_1	$V_{rot,1}$ km/sec	$V_{rot,2}$ km/sec
a												
Case 1	0.0000	2.777	9.000	6.000	3.639	4.385	3.077	4.287	0.2800	0.2800		
Case 2	0.0000	2.776	9.000	6.000	3.629	4.381	3.055	4.280	0.2800	0.2800	68.66	56.39
b												
Case 1	2.6725	2.737	8.929	5.994	3.959	4.285	3.110	4.267	0.8744	0.2800		
Case 2	2.6267	2.743	8.939	5.995	3.914	4.295	3.085	4.265	0.8247	0.2800	143.69	63.39
c												
Case 1	2.6854	3.190	5.314	9.608	3.457	4.120	3.811	4.396	0.8799	0.2801		
Case 2	2.6329	3.192	5.318	9.616	3.264	4.135	3.834	4.406	0.8267	0.2801	121.81	67.59
d												
Case 1	3.0784	11.743	2.727	12.168	3.776	4.128	4.145	4.461	0.9800	0.5892		
Case 2	3.3567	7.213	3.388	11.497	3.442	4.162	4.123	4.405	0.9800	0.3481	58.41	41.79
e												
Case 1	3.0941	32.534	1.797	13.082	3.959	4.028	4.276	4.539	0.9799	0.8775		
Case 2												
f												
Case 1	3.1484	42.382	1.572	13.245	3.186	4.775	4.308	4.549	0.8856	0.8793		
Case 2	3.5470	32.531	1.714	13.037	3.280	4.686	4.308	4.419	0.9800	0.8261	0.97	10.74

**Fig. 1.** Surface rotating velocity distribution of primary varying with time. Four panels (a), (b), (c), and (d) correspond to periods: 2.776, 2.760, 2.746, and 2.628 days, and corresponding evolutive time is 0, 2.3386×10^7 , 2.6194×10^7 , 2.6287×10^7 yrs, respectively.

$\theta = \frac{\pi}{2}$; $\varphi = k\pi + \frac{\pi}{2}$, $k = 0, 1$ and reaches the secondary maximal value of 1.2445 at the point of $\theta = \frac{\pi}{2}$; $\varphi = k\pi$, $k = 0, 1$. The results show that the effect produced by tidal distortion is lower in comparison with what is produced by rotational distortion on the equatorial plane. However, with the mass conversion, the op-

posite situation can emerge. It is concluded that tidal distortions are related to the mass ratio of the secondary to the primary. These results suggest that rotation and tide have strong influences on the stellar surface. They modify the gravity and change the spherically-symmetric shape into the triaxial ellipsoid shape.

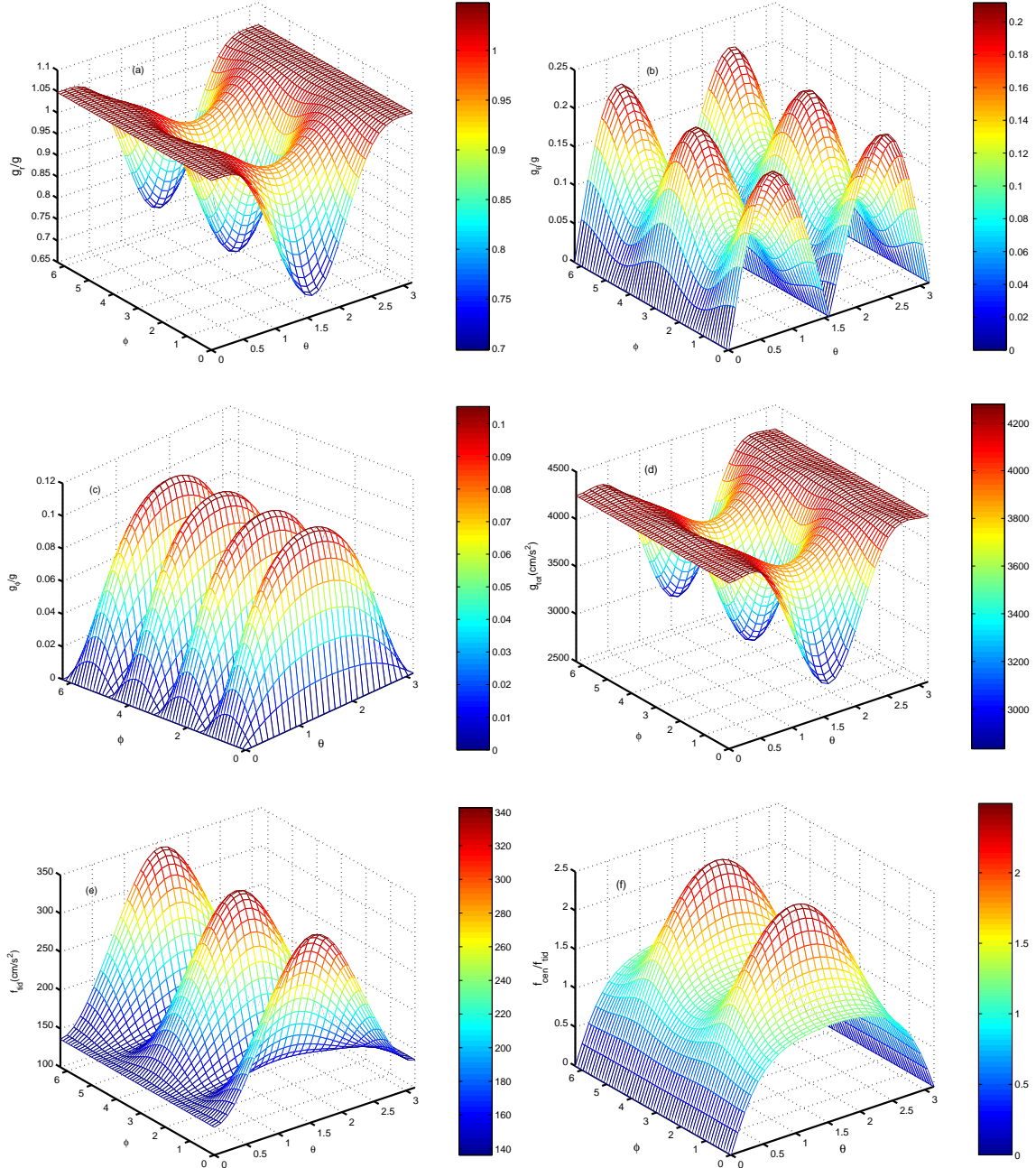


Fig. 2. Variation of relative gravitational accelerations at the surface of primary under coordinate θ and φ as mass overflow begins. The quantities g_r , g_θ , and g_φ are the three components of the gravitational acceleration g_{tot} . Quantity g equals the gravitational acceleration of the corresponding equivalent sphere ($g = \frac{GM}{r_p^2}$).

Furthermore, the stellar structure equations are basically revised due to the distribution of the relative quantity in the outer region.

According to the Von Zeipel theorem, the mass loss due to stellar winds should be proportional to local effective gravity. Polar ejection is intensified by the tidal effect. The higher gravity at the peak of the axis b makes it hotter. The ejection of an equatorial ring may be favoured by both the opacity effect and the higher temperature at the peak of the semi-axis b . This effect is called the $g_e(\theta, \varphi)$ -effect in this paper. It is predicted that the $g_e(\theta, \varphi)$ -effect is as important as the g_e -effect suggested by Maeder (1999) and Maeder & Desjacques (2001). The shapes of planetary nebulae that deviate from spherical symmetry (ax-

isymmetrical one in particular) are often ascribed to rotation or tidal interaction (Soker 1997). Frankowski and Tylenda (2001) suggest that a mass-losing star can be noticeably distorted by tidal forces, thus the wind will exhibit an intrinsic directivity and may be globally intensified. Interestingly enough, the group of the B[e] stars shows a two-component stellar wind with a hot, highly ionized, fast wind at the poles and a slow, dense, disk-like wind at the equator (Zickgraf 1999). Maeder and Desjacques (2001) have noticed that the polar lobes and skirt in η Carinae and other LBV stars may naturally result from the g_{eff} and κ -effects. Langer et al. (1999) have shown that giant LBV outbursts depend on the initial rotation rate. Tout and Eggleton (1988) pro-

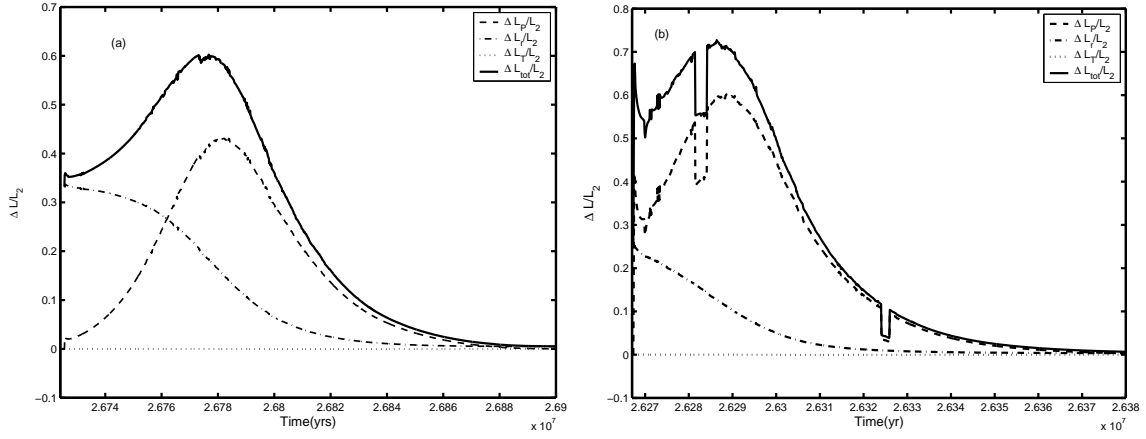


Fig. 3. Time variation of relative accretion luminosity at semi-detached stage. Panel (a) represents case 1 and panel (b) represents case 2. The solid, dotted, dashed and dotted-dashed curves correspond to the relative accretion luminosity with respect to total, thermal, potential and irradiative energies, respectively.

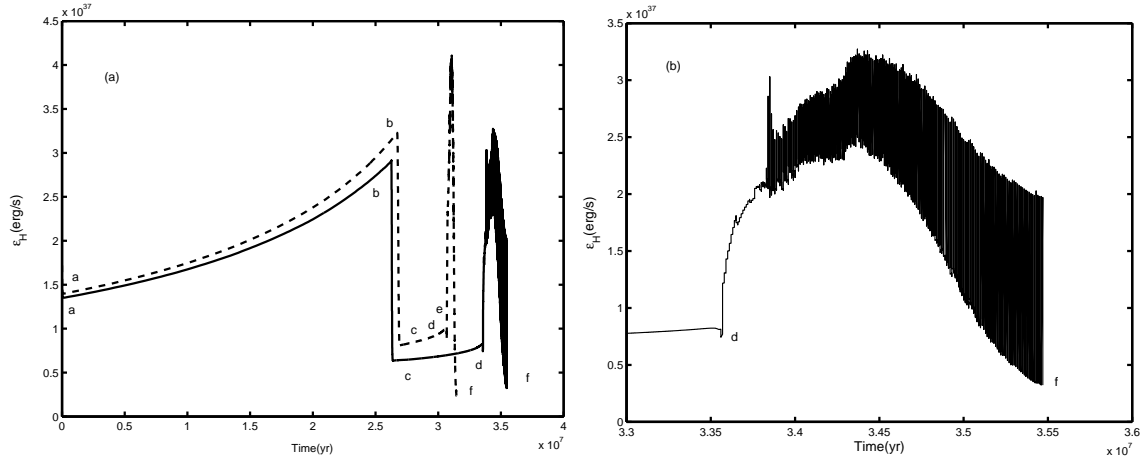


Fig. 4. Panel (a): variation in total H-burning generation energy rate in two cases. Panel (b): time variation in total H-burning generation energy rate in case 2 after main sequence. The solid curve represents case 2 and the dashed curve represents case 1.

posed a formula according to which the tidal torque would enhance the mass-loss rate by a factor of $1 + B \times \left(\frac{R}{R_{RL}}\right)^6$, where B is a parameter free to be adjusted (ranging from 5×10^2 to 10^4). Mass loss and associated loss of angular momentum are anisotropic in rotating binary stars. The theories for describing the mass loss and angular momentum loss from stellar winds should be altered partly in future work.

The time variation of relative accretion luminosity at the semi-detached stage is shown in Fig. 3. The two panels (a) and (b) correspond to cases 1 and 2, respectively. The figure shows that the release of transferred thermal energy approaches zero, which indicates that the transferred thermal energy can be ignored in the two cases. The irradiation energy plays an important role in the early stage of mass overflow and attenuates at the subsequent stage, which can be explained by the luminosity of the primary decreasing rapidly and the luminosity of the secondary increasing with mass transfer gradually. The transferred potential can exceed the irradiation energy as the mass transfer rate grows. The total accretion luminosity in case 2 is higher than the one in case 1 because the potentials in the two cases are different. From panel (b), it can be seen that the curve of the accretion luminosity fluctuates, indicating that the mass transfer process is unstable.

The total H-burning energy-generation rates of the primary in the two cases are shown in Fig. 4. Panel (b) shows the H-burning energy-generation rate in case 2 after the main sequence. From the difference between curves in panel (a), it is noticed that the effect of rotation causes the total H-burning energy-generation rate lower. As a result, the evolutive time in the main-sequence stage gets longer (cf. Table 1). Moreover, the larger fuel supply and lower initial luminosity of the rotating stars help to prolong the time which they spend on the main sequence (Heger & Langer 2000b). The lifetime extension in rotating binary star at the main-sequence stage can also be illustrated according to Suchkov (2001). Their results show that the age-velocity relation (AVR) between F stars in the binary system is different from the one between “truly single” F stars. The discrepancy between the two AVRs indicates that the putative binaries are, on average, older than similar normal single F stars at the same effective temperature and luminosity. It is speculated that this peculiarity comes from the impact of the interaction of components in a tight pair on stellar evolution, which results in the prolonged main-sequence lifetime of the primary F star. Moreover, no central helium-burning stage exists for case 2 (cf. Table 1). From panel (b), it can be seen that the energy-generation rate of the primary vibrates at the H-shell burning stage in case 2. These facts suggest that the

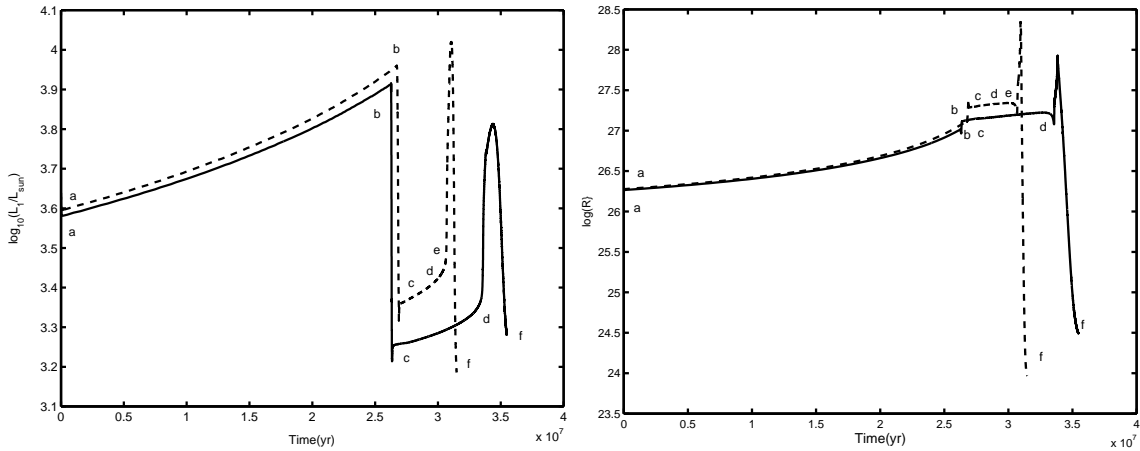


Fig. 5. Time-dependent variation in luminosity and equivalent radius of primary in two cases. The solid and dotted curves have the same meaning as in Fig. 4.

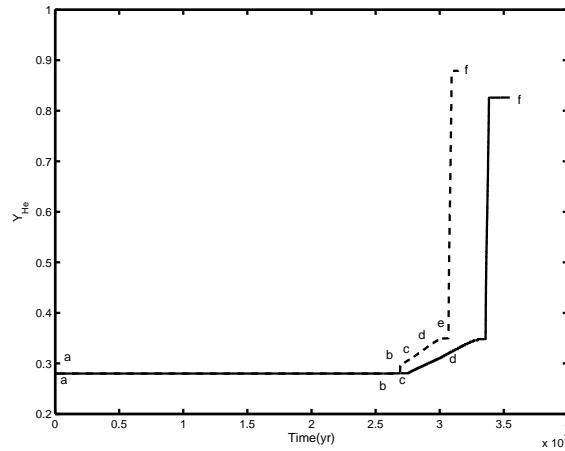


Fig. 6. Time-dependent variation in surface helium in two cases. The solid and dotted curves have the same meaning as in Fig. 4.

burning of H-shell is unstable in case 2. The reason lies in the centrifugal force reducing the effective gravity at the stellar envelope. The luminosity and surface temperature there decrease (Kippenhahn 1977; Langer 1998; Meynet and Maeder 1997). Thus, the shell source becomes cooler, thinner, and more degenerated as the He core mass increases. As the hydrogen shell becomes unstable, the thickness $\frac{D}{r_s}$ and surface temperature are ~ 0.203 and $1.1885 \times 10^4 K$, respectively. This physical condition leads to thermal instability (Yoon et al., 2004), and the H-shell source experiences slight oscillation. It is well known that the energy-generation rate is proportional to temperature and density ($\epsilon \propto \rho T^n$); therefore, the curve of the H-shell energy-generation rate fluctuates.

The time-dependent variation in the luminosity and the equivalent radius of the primary in the two cases are illustrated in Fig. 5. Because the rotating star has a lower energy-generation rate, the luminosity of the primary is lower, which is the consequence of decreased central temperature in rotating models due to decreased effective gravity (Meynet and Maeder 1997). Then, the primary expands slowly in case 2. It is observed that case 1 reaches point b at $t = 2.6725 \times 10^7 yr$, while case 2 reaches point b at $t = 2.6267 \times 10^7 yr$. The initiation time of mass transfer for case 2 is advanced by about $\sim 1.71\%$. Similarly, numerical calculation by Petrovic et al. (2005b) shows the radius of the rotating primary increases faster than that of the non-rotating primary due to the influence of centrifugal forces. Their results also

show that mass transfer of Case A starts earlier in rotating binary system, which is consistent with ours. If the rotating star is still treated as a spherical star, the initiation time of mass overflow should be later than that in the non-rotational case. Actually, because of the distortion by rotation and tide, the time for mass overflow may be extended. Therefore, it is very important to investigate distortion in close binary systems.

The time-dependent variation in the helium compositions at the surface of the primary is illustrated in Fig. 6. The H-shell burning begins at $t = 2.6854 \times 10^7 yr$ in case 1 while at $t = 2.6329 \times 10^7 yr$ in case 2 (cf. Table 1). Therefore, the initiation time of H-shell burning is advanced by $1.71 \times 10^5 yr$. Moreover, the helium composition at the surface of the primary is 0.280051 at point c, suggesting that the diffusion process progresses slowly in a rotating star. Cantiello et al. (2007) also indicate that rotationally induced mixing before the onset of mass transfer is negligible, in contrast to typical O stars evolving separately; hence, the alteration of surface compositions depends on both initial mass and rotation rates. The sample of the OB-type binaries with orbital periods ranging from one to five days by Hilditch et al. (2005) shows enhanced N abundance up to 0.4 dex. Langer et al. (2008) have discovered that for the same binary system, but with the initial period of six days instead of three days, its mass gainer is accelerated to a rotational velocity of nearly $500 km s^{-1}$, which produces an extra nitrogen enrichment from more than a factor two to about 1 dex in total.

Because there is no central helium-burning phase for case 2, the diffusion process can be neglected in the interior region of the primary after the main sequences.

4. Conclusions

The main achievements of this study may be summarised as follows.

(a) The distortion throughout the outer layer of the primary is considerable. The detailed theoretical models that investigate the outer regions of the two components have deviated somewhat from the lowest approximation of the Roche model. The high-order perturbing potential is required especially in the investigation of the evolution of short-period binary system.

(b) The equilibrium structures of distorted stars are actually triaxial ellipsoids. A formula describing rotationally and tidally distorted stars is presented. The shape of the ellipsoid is related to the mean density of the component and the potentials of centrifugal and tidal force.

(c) The radial components of the centrifugal force and the tidal force cause the variation in gravitation. The tangent components of the centrifugal force and the tidal force cannot be equalized and, instead, they change the shapes of the components from perfect spheres to triaxial ellipsoids. Mass loss and associated angular momentum loss are anisotropic in rotating binary stars. Ejection is intensified by tidal effect. The ejection of an equatorial ring may be favoured by both the opacity effect and the higher temperature at the peak of semi-axis b . This effect is called the $g_e(\theta, \varphi)$ -effect in this paper.

(d) The rotating star has an unstable H-burning shell after the main sequence. The components expand slowly due to their lower luminosity. If the components are still treated as spherical stars, some important physical processes can be ignored.

Acknowledgements. We are grateful to Professor Norbert Langer and Dr. Stéphane Mathis for their valuable suggestions and insightful remarks, which have improved this paper greatly. Also we thank Professor Norbert Langer for his kind help in improving our English.

References

- Baker, N. 1966, in *Stellar Evolution*, ed. R. F. Stein, & A. G. W. Cameron (Plenum, New York) 333
- Burša, M., 1988, *Bull. Astron. Inst. Czechosl.* 39, 289
- Burša, M., 1989a, *Bull. Astron. Inst. Czechosl.* 40, 125B
- Cantiello, M., Yoon, S.-C., Langer, N., & Livio, M. 2007, *A&A*, 465, L29
- Chan, K.L., Chau, W.Y., 1979, *ApJ*, 233, 950
- Chandrasekhar, S.; 1933, *MNRAS*, 93, 390
- Charbonnel, C., 1994, *A&A*, 282, 811
- Charbonnel, C., 1995, *ApJ*, 453, L41
- Charboyer, B., & Zahn, J.-P. 1992, *A&A*, 253, 173
- De Greve J. P., 1993, *A&A*, 97, 527
- De Loore, C., 1980, *Space sci. Rev.*, 26, 113
- Decressin et al., 2009, *A&A*, 495, 271
- Denissenkov, P.A., Ivanova, N.S., and Weiss, A., 1999, *A&A*, 341, 181
- Eggleton, P.P., 1971, *MNRAS*, 151, 351
- Eggleton, P.P., 1972, *MNRAS*, 156, 361
- Eggleton, P.P., 1973, *MNRAS*, 163, 279
- Endal, A. S. & Sofia, S., 1976, *ApJ*, 210, 184
- Endal, A. S. & Sofia, S., 1978, *ApJ*, 220, 279
- Frankowski, A. & Tylenda, R., 2001, *A&A*, 367, 513
- Giuricin G., et al., 1984, *A&A*, 131, 152
- Georgy, C., Meynet, G. and Maeder, A., *Proc. IAU-Symp.*, No. 255, 2008, L. K. Hunt, S. Madden @ R. Schneider, eds., in press [astro-ph/08075061]
- Han, Z., Webbink, R.F., *A&A*, 1999, 236, 107
- Hilditch, R. W., Howarth, I. D., & Harries, T. J. 2005, *MNRAS*, 357, 304
- Heger, A., Langer, N. and Woosley, S.E., 2000a, *ApJ*, 528, 368
- Heger, A., Langer, N. 2000b, *ApJ*, 544, 1016
- Hofmeister, E., Kippenhahn, R., Weigert, A.: *Z.f. Astroph.* 59, p.215-241, 1964;
- Huang, R. Q., 2004a, *A&A*, 425, 591H
- Huang, R. Q., 2004b, *A&A*, 422, 981H
- Huang, R. Q., Taam, R. E., 1990, *A&A*, 236, 107
- Huang, R. Q., Yu, K.N., 1993, *A&A*, 267, 392
- Jackson, S.; 1970, *ApJ*, 160, 685
- kähler, H. A. & A., 2002, 395, 899 *Celestial Bodies* (The University of Wisconsin Press)
- Kippenhahn, R., Thomas, H. C., 1970, In: Slettebak A. (ed.), *Stellar Rotation*, D. Reidel Publ. Co. Dordrecht, Holland, p. 20
- Kippenhahn, R., Weigert, A., Hofmeister, E., 1967. In: *Computational methods in Physics*, Vol.7 Academic Press, New York, p.129
- Kippenhahn, R., Weigert, A., 1967, *ApJ*, 65, 251
- Kippenhahn, R., Meyer-Hofmeister, E., 1977, *A&A*, 54, 539K
- Kippenhahn, R., Weigert, A., 1990, in *Stellar Structure and Evolution* (Berlin: Springer Verlag), 468
- Kopal, Z., 1959, in *Close Binary systems*, (New York: Wiley)
- Kopal, Z., 1960, in *Figures of Equilibrium of Celestial Bodies* (The University of Wisconsin Press)
- Kopal, Z., *Adv. Astro. Astroph.*, 1972, 9, 1
- Kopal, Z., *Astroph. Spac Sci.*, 1974, 27, 389
- Landin, N. R., Mendes, L.T.S., Vaz, L.P.R., 2009, *A&A*, 494, 209
- Langer N. 1998, *A&A*, 329, 551
- Langer N. 1999, *A&A*, 346, 37L
- Langer N. 1999, *ApJ*, 520, L49
- Langer, N.; Yoon, S.-C.; Petrovic, J.; Heger, A. 2003 In *stellar Rotation*, *Proc. IAU-Symp.*, IN press..215 (San Francisco: ASP), ed. A. Maeder, P. Eenens, in press [astro-ph/0302232L]
- Langer N., Cantiello M., Yoon S.-C., Hunter I., Brott I., Lennon D.J., de Mink S.E., Verheijdt M., Invited review for *Proceedings of IAU-Symp. 250 on Massive Stars as Cosmic Engines*, F. Bresolin, P. Crowther & J. Puls, eds [astro-ph/08030621]
- Langer, N.; Heger, A., 1998, *ASPC*, 131, 76L
- Li L., Han Z., Zhang F., 2004a, *MNRAS*, 351, 137
- Li L., Han Z., Zhang F., 2004b, *MNRAS*, 355, 1388
- Li L., Han Z., Zhang F., 2005, *MNRAS*, 360, L372
- Maeder, A., Meynet, G., 2000, *ARAA*, 38, 143
- Maeder, A., 1997, *A&A*, 321, 134
- Maeder, A., Zahn, J.-P., 1998, *A&A*, 334, 1000
- Maeder, A., 1999, *A&A*, 347, 185
- Maeder, A., Desjacques, V., 2001, *A&AL*, 372, L9
- Matthews, L.D., & Mathieu, R.D. 1992, in *IAU Colloq. 135, Complimentary Approaches to Double and Multiple Star Research*, ed. H.A. McAlister & W.I. Hartkopf (ASP Conf. Ser. 32; San Francisco: ASP), 244
- Meynet, G., Maeder, A., 1997, *A&A*, 321, 465
- Meynet, G., Maeder, A., 2000, *A&A*, 361, 101
- Pinsonneault, M. H., Kawaler, S. D., Sofia, S., Demarque, P., 1989, *ApJS*, 338, 424
- Petrovic, J., Langer, N., Yoon, S.-C., Heger, A., 2005a, *A&A*, 435, 247
- Petrovic, J., Langer, N., van der Hucht, K. A. van der, 2005b, *A&A*, 435, 1013
- Renoizé, et al., 2002, *A&A*, 389, 485
- Rieutord, M., Zahn, J.-P., 1997, *ApJ*, 474, 760R
- Soker, N. 1997, *ApJS*, 112, 487
- Suchkov A. A., 2001, *A&A*, 369, 554
- Talon et al., 1997, *A&A*, 322, 209
- Tout, Ch. A., & Eggleton, P. P. 1988, *MNRAS*, 231, 823
- Vanbeveren D., 1991, *Space Sci. Rev.*, 56, 249
- Van Hamme W., Wilson R. E., 1990, *AJ*, 100(6), 1981
- von Zeipel H., 1924, *MNRAS*, 84, 665
- Yoon, S.-C., Langer, N. and Sluys, M. van der, 2004, *A&A*, 425, 207
- Yoon, S.-C., Langer, N. and Norman, 2006, *A&A*, 460, 199
- Zahn, J.-P. 1966, *AnAp*, 29, 489
- Zahn, J.-P. 1975, *A&A*, 41, 329
- Zahn, J.-P. 1977, *A&A*, 57, 383
- Zahn, J.-P. 1992, *A&A*, 265, 115
- Zahn, J.-P. 1997, *ApJ*, 474, 760R
- Zickgraf, F. J., 1999, *Lect. Notes Phys.*, 523, 40